Remote Sensing of Environment 234 (2019) 111440

Contents lists available at ScienceDirect

Remote Sensing of Environment

journal homepage: www.elsevier.com/locate/rse

Volcanic structures investigation through SAR and seismic interferometric methods: The 2011–2013 Campi Flegrei unrest episode

S. Pepe[a], L. De Siena[a,b], A. Barone[a,c], R. Castaldo[a], L. D'Auria[d], M. Manzo[a], F. Casu[a], M. Fedi[c], R. Lanari[a], F. Bianco[e], P. Tizzani[a,*]

[a] Consiglio Nazionale delle Ricerche (CNR) of Italy, Istituto per il Rilevamento Elettromagnetico dell'Ambiente (IREA), via Diocleziano 328, 80124, Napoli, Italy
[b] Institute of Geosciences, Johannes Gutenberg University, J.-J.-Becher-Weg 21, D-55128, Mainz, Germany
[c] Department of Earth, Environmental and Resources Science, University of Naples "Federico II", Monte Sant'Angelo (L building), Via Cinthia 21, 80126, Napoli, Italy
[d] Istituto Volcanòlogico de Canarias, 38320, San Cristóbal de La Laguna, S/C de Tenerife, Spain
[e] Istituto Nazionale di Geofisica e Vulcanologia, Sezione Osservatorio Vesuviano, Via Diocleziano 328, 80124, Napoli, Italy

ARTICLE INFO

Keywords:
InSAR
Ambient noise tomography
Total horizontal derivative
Campi Flegrei caldera
Natural seismicity

ABSTRACT

Observations from satellites provide high-resolution images of ground deformation allowing to infer deformation sources by developing advanced modeling of magma ascent and intrusion processes. Nevertheless, such models can be strongly biased without a precise model of the internal structure of the volcano. In this study, we jointly exploited two interferometric techniques to interpret the 2011–2013 unrest at Campi Flegrei caldera (CFc). The first is the Interferometric Synthetic Aperture Radar (InSAR) technique, which provides highly-resolved spatial and temporal images of ground deformation. The second is the Ambient Noise Tomography (ANT), which images subsurface structures, providing the constraints necessary to infer the depth of the shallow source at CFc (between 0.8 and 1.2 km). We applied for the first time a tool to delineate the deformation source boundaries from the observed deformation maps: the Total Horizontal Derivative (THD) technique. The THD processes the vertical component of the ground deformation field detected through InSAR applied to COSMO-SkyMed data. The patterns retrieved by applying the THD technique show consistent spatial correlations with (1) the seismic group-velocity maps achieved through the ANT and (2) the distribution of the earthquakes nucleated during the unrest at ~1 km. High-velocity anomalies, the retrieved geometrical features of the deformation field, and the spatial distribution of seismicity coincide with extinct volcanic vents in the eastern part of the caldera (Solfatara/Pisciarelli and Astroni). Such a coincidence hints at a significant role of the extinct plumbing system in either constraining or channeling the eastward propagation of magmatic fluids. Here, we demonstrated that a joint analysis of the InSAR patterns, seismic structures, and seismicity allows us to model in space and time the characteristics and nature of the shallow deformation source at CFc. Using published literature, we show that the effects of structural heterogeneities at shallow depths may have a more significant early-stage impact on the evolution of the surface displacement signals than deeper magmatic sources: these secondary structural effects may produce local amplification in the deformation records which can be mistakenly interpreted as early signals of impending eruptions. The achieved results are particularly relevant for the understanding of the origin of deformation signal at volcanoes where magma propagation within sills is expected, as at CFc.

1. Introduction

Volcanoes are an ideal environment to test the ability of both proximal and remote-sensing techniques to characterize the internal features of the volcanic feeding system, and to model their temporal evolution (Tizzani et al., 2010; Masterlark et al. 2012, 2016; Del Negro et al., 2013; Mattia et al., 2015; Castaldo et al., 2018a). Interferometric Synthetic Aperture Radar (InSAR) is a remote-sensing technology capable of imaging surface deformation over wide areas (Massonnet and Feigl, 1998; Franceschetti and Lanari, 1999; Bürgmann et al., 2000). In particular, InSAR exploits the phase difference (interferogram) between pairs of SAR images, collected over the same area at different epochs (temporal baseline) and with different orbital positions (spatial baseline). It provides a measurement of the ground deformation projected along the radar Line Of Sight (LOS), with a centimeter-to-millimeter accuracy (Gabriel et al., 1989). In the last decades, several

* Corresponding author.
E-mail address: tizzani.p@irea.cnr.it (P. Tizzani).

https://doi.org/10.1016/j.rse.2019.111440
Received 4 April 2019; Received in revised form 20 September 2019; Accepted 21 September 2019

InSAR algorithms have been developed to detect surface deformation and analyze their space-time characteristics using large stacks of SAR images acquired from different satellites. These approaches exploit long sequences of differential interferograms in order to generate time-series of the detected LOS-projected displacements for each coherent point (i.e., where the phase information is preserved - Ferretti et al., 2001; Mora et al., 2003; Hooper et al., 2014). Among these algorithms, the Small BAseline Subset (SBAS) approach (Berardino et al., 2002; Pepe et al., 2005) is well suited to resolve the space-time evolution of the surface deformation at volcanoes and it is currently employed to monitor volcanic activity worldwide (Lanari et al., 2002; Borgia et al., 2005; Fernandez al., 2009; Tizzani et al., 2009; Solaro et al., 2010; Tizzani et al., 2010; Tizzani et al., 2015; De Novellis et al., 2017; Castaldo et al., 2017; Pepe et al., 2017, 2018).

InSAR results (i.e., mean deformation velocities maps and the corresponding time-series) are used to infer the source and dynamics of deformation phenomena in volcanic areas. In particular, these models work well for bell-shaped deformation anomalies, typical for caldera floors like Long Valley and Yellowstone (Tizzani et al., 2007, 2009; 2015). In contrast, the relatively-simple models employed to infer the location and size of deformation sources suffer from major biases if pre-existing tectonic structures (Orsi et al., 1999), shallow horizontal interfaces (Vanorio et al., 2005) and/or cold magmatic intrusions (Chiodini et al., 2015) exist. These structural constraints modulate the ground deformation pattern (Trasatti et al., 2008; Amoruso et al., 2008; Manconi et al., 2010; D'D' Auria et al., 2015): without any constraint on the volcanic structures at depth, the geometry and the characteristics of the deformation sources may become uncertain, leading to incorrect interpretations of volcanic unrest from deformation data at the earlier stages of a volcanic crisis, when the signal-to-noise ratio is still low. For example, Del Gaudio et al. (2009) show that the first deformation signal during the 2005 CFc unrest was measured at Solfatara; only after a few days the deformation bell was centered on the primary deformation source offshore Pozzuoli.

Seismic tomography maps the Earth subsurface using seismic waves produced by active and passive sources and recorded at a seismic network. The derived seismic models of velocity or attenuation provide an image of structural, thermal, or compositional variations inside the Earth; in volcanoes, these tomographic models can constrain geodynamical and volcanological simulations (Masterlark et al., 2012; Reuber et al., 2018). At CFc, seismic tomography gives the structural constraints necessary to map fractures, interfaces, and older plumbing systems (Zollo et al., 2003; Vanorio et al., 2005; Battaglia et al., 2008; De Siena et al., 2010, 2017a; 2017b; Calò and Tramelli, 2018). The seismic tomography images of the onshore CFc mentioned above are built on seismic earthquake data recorded between 1982–84: they were thus an image of this period of unrest (Aster and Meyer, 1988). The maps show that, in 1982–84, a reservoir containing high-pressure fluids was repeatedly fractured by magmatic intrusions (Amoruso et al., 2008) and/or fluid injections (Vanorio et al., 2005) under the town of Pozzuoli (De Siena et al., 2017b). Since 1985, seismicity has mostly been limited to the shallow hydrothermal systems, progressively shifting towards the eastern side of the caldera (Di Luccio et al., 2015). The only seismic imaging available since 1985 was thus obtained in 2001 by using the active data of the SERAPIS seismic experiment, shot in the submerged center of the caldera (Zollo et al., 2003; Serlenga et al., 2016), at least until De Siena et al. (2018) published an Ambient Noise Tomography (ANT) of the caldera.

ANT is based on seismic interferometry measurements and has rapidly grown as a standard imaging (Shapiro et al., 2005; Brenguier et al., 2007) and monitoring (Lecocq et al., 2014) technique over the last 15 years. As standard travel-time tomography (e.g., Koulakov and Vargas, 2018), it has shown to be particularly useful in studying the structure and the dynamics of active volcanoes (Brenguier et al., 2007). This technique turns ambient noise recorded at two seismic stations into seismic signals propagating between them (Curtis et al., 2006). As for InSAR, the name interferometry refers to the phenomenon of interference. More precisely, scientists can reconstruct the Green's function, as the impulse was produced at one station and recorded at the other (Wapenaar and Fokkema, 2006). This response provides high quality seismic data for applying ANT in complex geological structures as volcanoes (Sens-Schönfelder and Wegler, 2006; Brenguier et al., 2007; Nagaoka et al., 2012; Obermann et al., 2013; Jaxybulatov et al., 2014; Garnier and Papanicolaou, 2016). With this technique, De Siena et al. (2018) have imaged the Rayleigh-wave velocity of the fluid feeder-pathway responsible for the 2011–2013 deformation unrest at CFc. The model shows-surface wave group velocities that are mostly consistent with the P- and S-wave velocity maps imaged during 1982–84, including the low-velocity fluid storage zone under Pozzuoli (Vanorio et al., 2005) and high velocity anomalies underlining the caldera rim (Battaglia et al., 2008). The main difference between 2011–13 and 1982–84 is the presence of a high-velocity anomaly under Solfatara, at ~1.7 km which shifts towards Pisciarelli at ~1 km and disappears at shallower depths. This is the first tomographic image of the onshore caldera since 1984, therefore the first that can be used in conjunction with InSAR data.

In the present study, we also use earthquake locations detected between 2005 and 2016. The earthquakes were recorded by the permanent seismic networks of Osservatorio Vesuviano - Istituto Nazionale di Geofisica e Vulcanologia (INGV). The nucleation of micro-earthquakes and the spatial cutoff at depth are strongly linked to the rheological stratification of the crust beneath the CFc (Castaldo et al., 2018a). We stress that the seismicity currently recorded at CFc is too low in magnitude and sparse to apply local earthquake tomography (D'Auria et al., 2011). On September 7th' 2012 a deep seismic swarm, possibly of magmatic origin, occurred during the rapid uplift event (2012–2013). This seismic activity diverged from the last 28 years almost exclusively driven by shallow hydrothermal processes (D'D' Auria et al., 2015). Ground deformation observed in 2012–13 derived through satellite interferometry and GPS measurements has previously been interpreted as resulting from a magmatic sill intrusion of $0.0042 \pm 0.0002\,km^3$ at shallow depth ($3090 \pm 138\,m$) (D'D' Auria et al., 2015), whose location agrees with the low-velocity zone imaged by ANT at a depth of ~2 km (De Siena et al., 2018).

In the present study, SAR and ANT maps obtained between 2011 and 2013 provide dynamic and structural information that can be jointly used to interpret the deformation processes. While the former allows identifying the deformation source boundaries laterally and/or the involved volcanic structures that modulate the observed deformation pattern, the latter yields a velocity model characterizing the structure of the volcano in 3D. The comparison of these results with the 2005–2016 earthquake locations highlights the volume where the stresses were concentrated, confirming that the caldera structures play an active role in modulating the deformation signals.

2. Data and methods

2.1. SAR interferometry

We apply the Small BAseline Subset (SBAS) approach (Berardino et al., 2002; Pepe et al., 2005) to detect and follow the temporal evolution of the surface deformation affecting CFc during the time interval of interest. To this aim, we process the SAR data acquired from the Italian COSMO-SkyMed constellation along ascending and descending orbits. Specifically, we processed 215 ascending and 46 descending SAR data[1] relevant to the February 2011–January 2014 time-interval, and

[1] We remark that the temporal sampling for the descending orbits is significantly poorer than the ascending one (46 images vs 215 images); this is due to the SAR data acquisition policy of the COSMO-SkyMed mission, which does not necessarily guarantee the collection of SAR images in the same conditions

computed about 750 interferograms from the ascending orbits and 102 from the descending ones (selected by imposing maximum perpendicular and temporal baseline values of 800 *m* and 400 days, respectively). The interferograms were inverted by applying the above mentioned SBAS-InSAR technique to generate mean deformation velocity maps (Fig. 1a and b) and the corresponding time-series. The achieved results were computed on an output grid with 30 m × 30 *m* spatial resolution and are referred to a reference pixel in the center of the city of Naples.

The availability of InSAR measurements for both the ascending and descending radar LOS (Fig. 1a and b) allows discriminating the Vertical (V) and East–West (E-W) mean velocity components (Fig. 1c and d) (Wright et al., 2003; Manzo et al., 2006). Moreover, due to the non-uniform temporal sampling, the ascending and descending data were resampled to 11 days by using a linear interpolation (Del Negro et al., 2013). This allowed the computation of time-series pairs representing the temporal evolution of the E-W and Vertical deformation components (Fig. 1e–g).

In addition, we show that both the ascending and descending LOS mean-deformation velocity maps record a maximum of about 6 cm/year at the Pozzuoli harbor, with the velocity pattern accommodated within the caldera boundaries. Fig. 1c and d depicts the vertical and E-W components of the mean velocity field, respectively. The first reveals an extended deformation pattern that involves the whole caldera, the latter the presence of a region of very-low velocity that separates the eastern and western sides of the caldera. Three pixels were selected to represent the Vertical and E-W components (Fig. 1e–g) and they are located within the caldera (P1 in Fig. 1c, P2 and P3 in Fig. 1d). Note that the vertical component of the ground deformation reaches a maximum value of about 18 cm (plot of Fig. 1e), while the horizontal displacements towards East and West reach maximum values of 8 cm (plot of Fig. 1f) and about 6 cm (plot of Fig. 1g), respectively.

Moreover, the vertical displacement in Pozzuoli shows three nearly-linear deformation trends (point P1 in Fig. 1e): step 1 (from February 2011 to May 2012) and step 2 (from May 2012 to April 2013) display positive deformation rates of about 4.8 cm/yr and 13 cm/yr respectively, while step 3 (April 2013 to January 2014) shows no relevant deformation. P1 has a maximum vertical displacement of about 6 cm, while later in the second step, the cumulative vertical displacement is about 18 cm.

Here, we use the *Total Horizontal Derivative (THD)* technique to perform a basic detection of the deformation source boundaries; we remark that the THD technique is an edge detection filter commonly employed for analyzing potential field data (Blakely, 1996; Florio et al., 1999) and it is based on analyzing the maxima of the horizontal gradient magnitude, as computed from the first order *x*- and *y*-derivatives of the field; their distribution depends on the source geometry since the maxima occur where the physical property has the greatest variation, that is at the boundaries of the sources. This is also true for higher-order field derivatives of related quantities such as the enhanced horizontal derivative method (Fedi and Florio, 2001; Luiso et al., 2018). In particular, the maxima horizontal gradient magnitude matches with the physical edges of the source (Blakely, 1996). Despite some limitations in its applicability and accuracy (Blakely, 1996), it is a powerful boundary analysis technique.

Following Castaldo et al. (2018b), we apply for the first time the THD algorithm to the vertical deformation at CFc. This technique provides reliable results, in the case of abrupt lateral contrasts of the investigated property (Blakely, 1996), typical of volcanic areas.

The THD_w for the vertical deformation is defined here as:

$$THD_w = \sqrt{\left(\frac{\partial w(x, y, z)}{\partial x}\right)^2 + \left(\frac{\partial w(x, y, z)}{\partial y}\right)^2} \quad (1)$$

where $w(x, y, z)$ represents the vertical component of the ground deformation at spatial coordinates (x, y, z). The horizontal derivatives are calculated using simple finite-difference relationships. To correctly examine the THD_w, the data have to be referred to the same *z*-level; thus, we performed the computation after reducing the vertical ground deformation component to a constant level (Castaldo et al., 2018b; Barone et al., 2019) by using a CWT (Continuous Wavelet Transform)-domain algorithm (Ridsdill-Smith, 1999). Note that the THD_w maxima allow to detect the boundaries of magmatic reservoirs and/or the volcanic structures that modulate the observed deformation patterns.

2.2. Seismic interferometry

Ambient Noise Tomography (ANT) uses the ambient seismic noise wave fields continuously recorded at a seismic network to image seismic wave velocities, without the use of earthquakes or artificial explosions (Shapiro et al., 2005). Depending on the scale and the ambient-noise source distribution, this technique analyzes noise time series (Fig. 2a) that span hours to years. The noise time series recorded at positions x_1 and x_2 ($n(x_1,t)$ and $n(x_2,t)$) are the superposition of noise source fields (Fig. 2b); their correlation gives the Green's function (G – i.e. the response of the medium to a source located at one of the stations) between x_1 and x_2 plus its time-reversed version (Fig. 2c), convolved with the autocorrelation of the noise[2] $S_N(t)$ (Wapenaar and Fokkema, 2006):

$$\{ G(x_1, x_2, t)+G(x_2, x_1, -t)\} * S_N(t) = < n(x_2, t) * n(x_1, -t)> \quad (2)$$

where * is the convolution operator.

We remark that the ensemble averaging ($< >$) in eq. (2) is replaced, in real case studies, by the integration over a sufficiently long time. Since the cross-correlation operation basically reconstructs an interferogram, the technique is also commonly referred to as “seismic interferometry”. In practice, the noise recorded by the station mainly comprises Rayleigh waves. The technique thus retrieves the Rayleigh-wave that we would record at station x_2 if we would have a “source of Rayleigh waves” at station x_1 plus its time reverse (Curtis et al., 2006). We also underline that eq. (2) is theoretically valid only in the case of uncorrelated and isotropic noise. For seismic periods between 1s and 2s, ambient noise sources at CFc are produced in the sea, with the direction of seismic energy perpendicular to the coastline (Fig. 2b) (Ardhuin et al., 2011). While these noise sources are far from being isotropic at CFc, especially along the SN direction, a careful selection of waveforms and appropriate processing allows the retrieval of the main surface-wave mode (De Siena et al., 2018). We stress that previous tomographic images of the onshore Campi Flegrei caldera were so far dependent on the seismicity recorded between 1982 and 1984: they were thus an image of this period of unrest.

The signals reported in Fig. 2c were recovered by cross-correlating the ambient noise recorded for at least 1 year at the temporary seismic stations of the Osservatorio Vesuviano - INGV during the CFc unrest of 2011–2013. Their causal and anti-causal components correspond to the surface-wave fundamental mode that would be recorded at a seismic station if the source of the surface waves was located at the other. The standard framework for surface-wave imaging employed by De Siena et al. (2018) picks the fundamental mode recovered at different periods (0.9 s, 1.2 s, 1.5 s and 2 s) and maps the surface velocity variations in space. The whole framework from seismic noise correlation to surface-

(*footnote continued*)
and with the same characteristics over time. This acquisition approach can limit the generation of long time-series of data, which are necessary for advanced InSAR applications.

[2] Here, we present a derivation of the connection between cross-correlation operation and Green function between stations in 1D. The surface-wave retrieval from ambient noise is a 2D problem but can be reduced to 1D in the case of isotropic noise sources, meaning equal illumination from all directions.

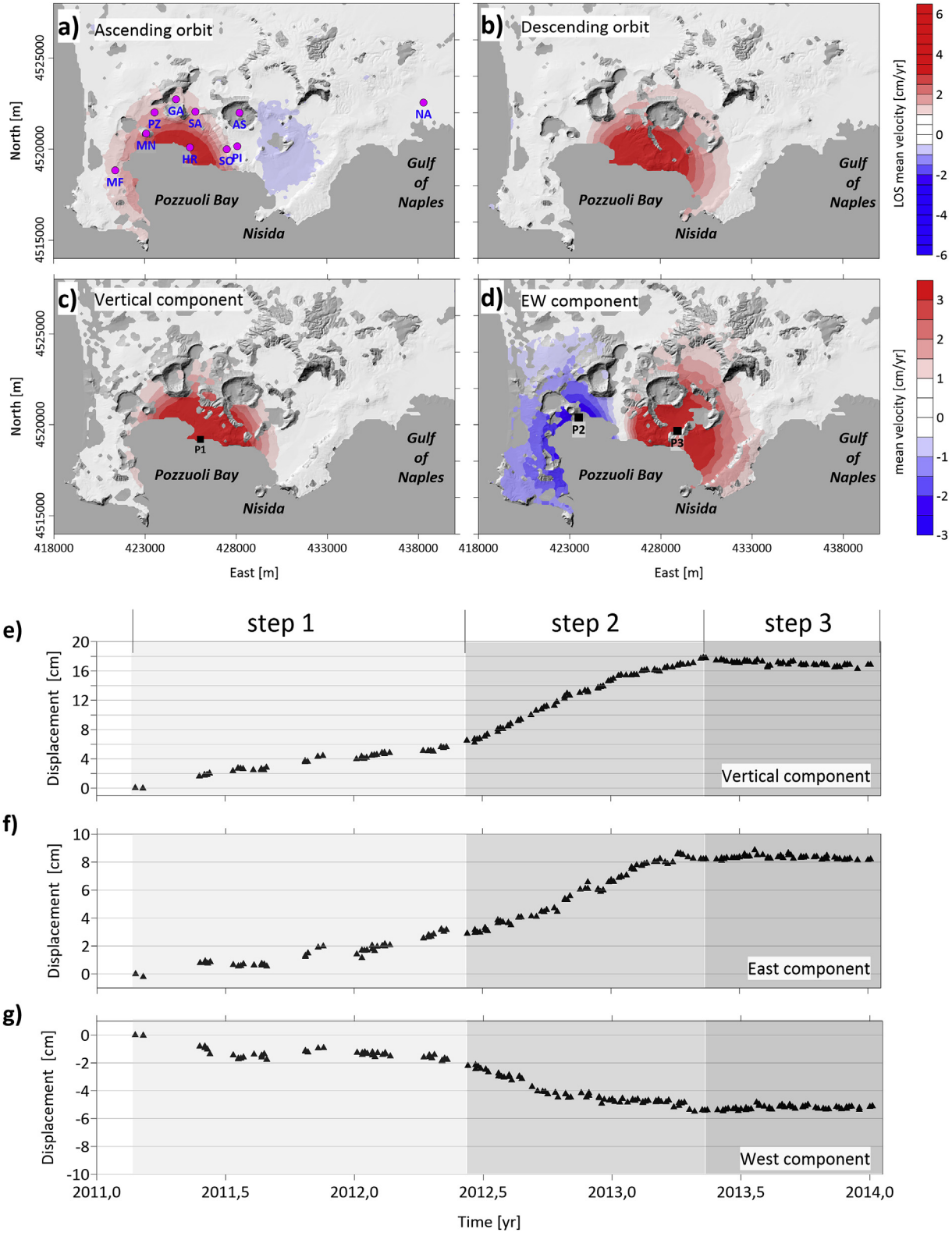

Fig. 1. SAR Interferometry. (a–b) Contour maps of the LOS mean deformation velocity, computed by applying the SBAS algorithm to the exploited COSMO-SkyMed ascending and descending SAR data processing the 2011–2013, respectively. (c–d) Contour maps of the Vertical and E-W mean deformation velocity components; P1, P2 and P3 identify three pixels located in the areas of maximum vertical (P1), western (P2) and eastern (P3) mean velocity. The magenta full circles represent the location of Pozzuoli site (PZ), Napoli city (NA) Monte Nuovo (NU), Pozzuoli Harbor (HR), Astroni crater (AS), Solfatara crater (SO), Pisciarelli fumarole spring (PI), Mount Gauro (GA) and San Vito (SA), Mofete (MF). All results are superimposed on the SRTM DEM of the area. (e–g) Vertical (P1) and East-West (P2 and P3) displacement time-series. The analyzed time period is divided in three steps (gray color regions) for different linear deformation trends analysis. (For interpretation of the references to color in this figure legend, the reader is referred to the Web version of this article.)

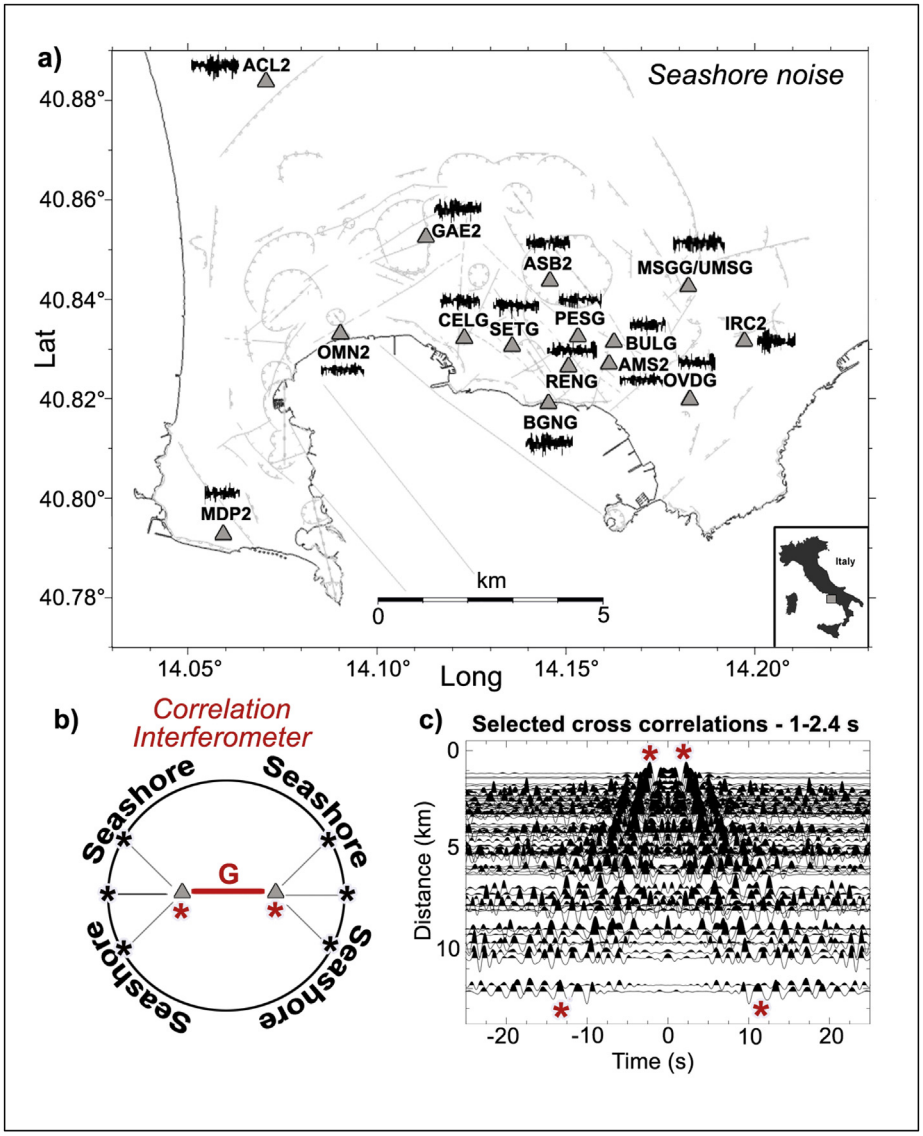

Fig. 2. Seismic Interferometry. Data and principles underlying seismic interferometry imaging during the 2011–2013 unrest: (a) seismic stations recorded a minimum of 1 year of ambient noise, whose sources are at the seashore; (b) cross-correlation of the simultaneous, uncorrelated, ambient-noise sources (black stars) propagating in opposite directions along the two-station line provides the Green's function (Earth response to an impulse) between the stations plus its time-reversed version. The cross-correlation effectively transforms each seismic station into a source of surface waves (red stars); (c) effective correlations (Green functions) retrieved from the noise dataset filtered between 1 and 2.4 s, shown for station pairs at increasing inter-station distances. The waves propagating at positive and negative relative times are the fundamental mode of a surface wave produced at a station and recorded at the other. (For interpretation of the references to color in this figure legend, the reader is referred to the Web version of this article.)

wave imaging is commonly known as ANT.

3. Results

The advanced InSAR measurements, specifically, the vertical and E-W displacements of the whole caldera relevant to the three identified temporal steps (see Fig. 1), are shown in Fig. 3. We observe that the E-W and Up-Down deformations drastically increase both spatially and in magnitude from step 1 to step 2 (Fig. 3a–d). The region of maximum vertical displacement corresponds to the area of lowest E-W deformation, particularly at step 2 (from May 2012 to April 2013), when the maximum deformation rate is recorded.

In order to investigate the volcanic source boundaries (i.e., possible magmatic reservoirs) and/or the involved structures that modulate the observed deformation pattern, we apply the THD technique to the displacement occurred during the second step. We first spatially regularize the dataset via ordinary kriging (Li and Heap, 2008), then we process the gridded vertical component by performing the constant level reduction at 200 m a.s.l. Finally, we compute the THD_w and analyze the spatial distribution of its maxima (Fig. 4), which is described by a bi-lobed shape having its axis of symmetry along the WNW-ESE direction. The alignment of the maxima is clearly defined to the east of Pozzuoli harbor, while the intensity of the maxima decreases in the western part of the caldera.

Fig. 5 shows the contour maps of the ANT group-velocity model obtained at periods 0.9 s (~0.9 km of depth), 1.2 s (~1 km of depth) and 2 s (~1.7 km of depth) by De Siena et al. (2018). The depths were inferred by using the 1D velocity model of Battaglia et al. (2008), while the seismic model has low-to-none resolution in shaded areas. Low-velocity anomalies comprise the western part of the metropolitan area of Naples at all depths (east in Fig. 5) and are likely due to caldera infills. High-velocity anomalies follow the caldera rim and contour low velocities to the west, NW, and NE, in correspondence to extinct vents active during the last 15 ka (Vilardo et al., 2010; Vitale and Isaia, 2014). The lowest velocities are centered between Pozzuoli, Monte Nuovo and Monte Gauro and describe an approximate circular shape at 2 s: at this period, a prominent high-velocity anomaly appears outside of the rim, just south of Solfatara, beneath younger vents (> 5 ka). The 2-s low-velocity anomaly has been interpreted by De Siena et al. (2018) as a “feeder-pathway” allowing for the migration of hot fluids to the upper structures of the volcano. These fluids migrate from west to east, following the shift in the center of the low-velocity anomaly. Moreover, this shift is paired by the migration towards east (1.2 s), and disappearance (0.9 s) of the Solfatara high-velocity anomaly. The 2011–2016 seismicity distribution highlights the area where the main stress was released during the crisis. In Fig. 6a, we show the seismicity

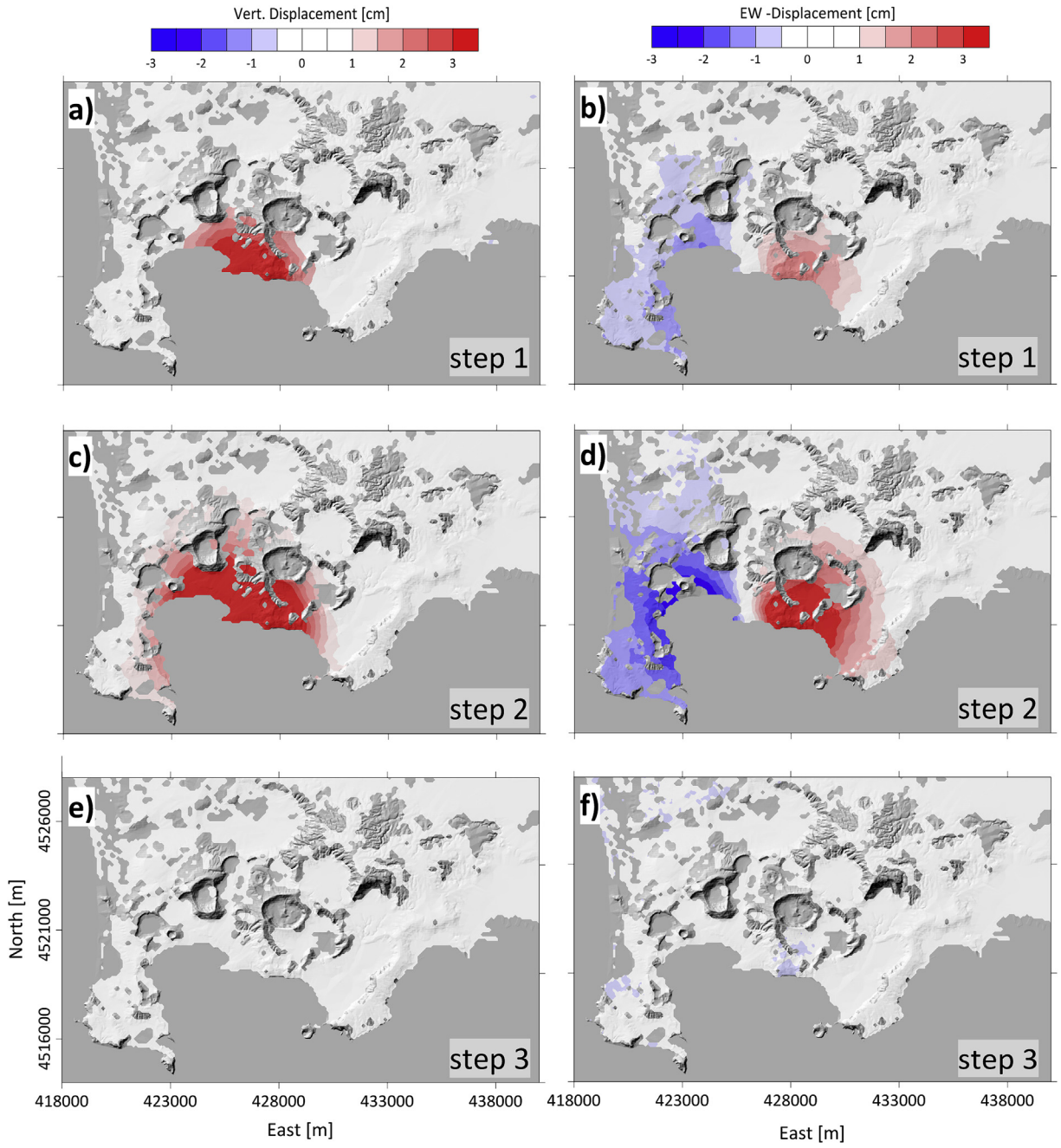

Fig. 3. InSAR analysis relevant to the investigated steps. (a, b) Contour maps of the vertical and E-W displacements, respectively, measured during the step 1 (reported in Fig. 1): Feb. 2011–May 2012, (c, d) the step 2 (reported in Fig. 1): May 2012–April 2013, and (e, f) the step 3 (reported in Fig. 1): April 2013–Jan. 2014. All results are superimposed on the SRTM DEM of the area.

divided in three periods, taking into account the same time intervals identified within the SAR interferometry analysis (Fig. 1).

4. Discussion

The joint analysis of InSAR and seismic interferometry results provides further insight into how geological structures modulate the deformation processes of the CFc caldera. The comparison of the THD_w maxima computed from the ground deformation measurements with the contrasts in the ANT group-velocity model (between 0.8 and 1.1 km/s) of different periods (0.9 s, 1.2 s and 2 s) indicates that the best spatial correlation is obtained at 1.2 s (i.e., depths of about 1 km). Both the THD and ANT analyses resolve the same bi-lobed feature with an axis of symmetry along the WNW-ESE direction (Fig. 6b). The distribution of the THD_w maxima intensifies toward the East of Pozzuoli and is paired by an increased group-velocity contrast of the eastern lobe (Fig. 6b). A good spatial correlation between the THD_w maxima and the ANT velocity contrasts is also found in the region at West of the Pozzuoli but this contrast is aseismic (Fig. 6a) except for the 2012 deeper swarm (D'D' Auria et al., 2015).

4.1. Eastern caldera

The eastern THD_w maxima and the achieved ANT velocity contrasts intersect a significant hydrothermal vent near Pisciarelli, which activated in 2013 (Chiodini et al., 2015). Sparse background seismicity between 2005 and 2016 is spread throughout the eastern CFc; however, earthquakes located at a depth of 1 ± 0.2 km (i.e., ANT 1.2 s period)

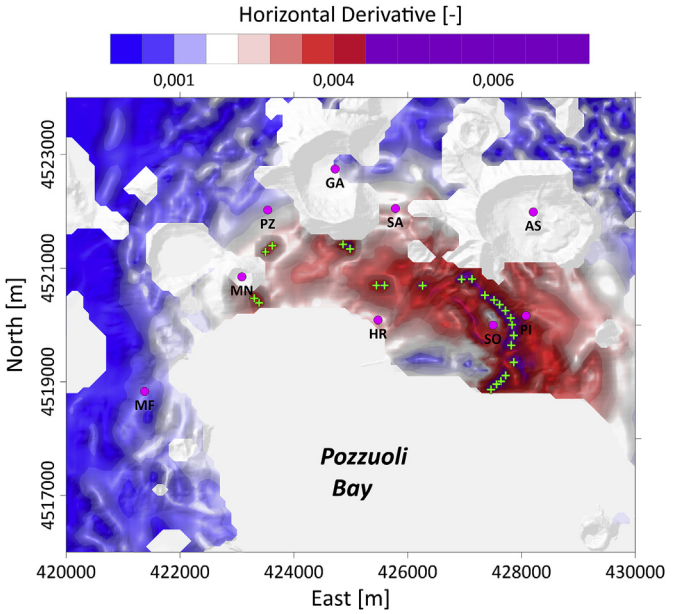

Fig. 4. THD analysis of the temporal step 2. a) THD_w results of the deformation related to step 2 (May 2012–April 2013). The green crosses identify the maxima of the THD. The magenta circles represent the location of Pozzuoli site (PZ), Napoli city (NA) Monte Nuovo (NU), Pozzuoli Harbor (HR), Astroni crater (AS), Solfatara crater (SO), Pisciarelli fumarole spring (PI), Mount Gauro (GA), Mofete (MF) and San Vito (SA). The results are superimposed on the SRTM DEM of the area. (For interpretation of the references to color in this figure legend, the reader is referred to the Web version of this article.)

are predominantly concentrated under Pisciarelli, just east of the boundary retrieved by THD and ANT technique (Fig. 6b). The most relevant aspect of our study is thus that the eastern structure lineaments detected by the ANT at 1 km of depth are the only dynamically-active structures in the considered period, as they show (1) high rates of the ground deformation (see THD_w maxima) and (2) earthquakes concentrated on the eastern side of the THD_w maxima (Fig. 6b).

These high velocity contrasts and high values of THD_w (corresponding to the boundaries of the source of deformation) mark the secondary deformation source (depth of ~1 km) modelled by Amoruso et al. (2014) at Solfatara/Pisciarelli (Fig. 4). This region of secondary deformation and seismicity corresponds to volcanic vents last active in 1982–84 (Vilardo et al., 2010; Vitale and Isaia, 2014; De Siena et al., 2017b). We infer that during the 2011–2013 unrest the shallower secondary source of deformation and seismicity recorded at Solfatara is the result of a structural effect, triggered by pressure/thermal gradient (Chiodini et al., 2015) and induced stress produced by the primary deformation source (Amoruso et al., 2014). The structures modulating stress, secondary deformation, and seismicity, are likely those in the shallower part of the high-Vp (> 4.4 km/s), low Vp/Vs (< 1.45) and low-scattering body recently imaged by Calò and Tramelli (2018) under the eastern sector of the caldera.

Several authors have shown the significant role played by pre-existing tectonic structures (Orsi et al., 1999; Trasatti et al., 2008; Manconi et al., 2010), horizontal interfaces (Amoruso et al., 2014; D'D' Auria et al., 2015; Vanorio et al., 2005) and/or cold magmatic intrusions (Chiodini et al., 2015) on the modulation of the ground deformation pattern at CFc. This role is confirmed by our maps and becomes crucial to understand the stress variations due to magmatic intrusion within sills (Amoruso et al., 2014), contributing to the dynamic assessment of vent opening probability at CFc (Giudicepietro et al., 2016). The spatial distribution of the anomalies (Fig. 6b) indicates that these shallower structures are able to channel fluids in the Solfatara/Pisciarelli area, where they produce stress and propagate to surface along almost-vertical structures.

This inference is supported by the high-resistivity vertical plume recently imaged by audiomagnetotellurics studies under Solfatara; this plume coincides with the boundaries retrieved by THD and ANT techniques, with the 1 km seismicity concentrated east of it. In this scenario, the source boundaries at depth overlap to the pre-existing tectonic structures due to the magma and/or hydrothermal fluids predisposition to fill the voids during the unrest events. The fluids travel from the central feeder-pathway through the fractures to the eastern part of the caldera; here, they are ultimately channeled by the high-velocity structures to (1) activate vents at the end of the unrest (Pisciarelli-Fig. 5); (2) produce the vertical high-resistive plume; (3) enhance the secondary deformation source depicted by the THD analysis (Amoruso et al., 2014). In summary, our results and published literature depict Solfatara as an almost-vertical very-low rigidity, low-velocity, highly-fractured zone (D'D' Auria et al., 2015; Di Luccio et al., 2015; Isaia et al., 2015), dynamically stressed from the west or SW at least since the 1982–1984 crisis (De Siena et al. 2017a,b).

4.2. Offshore and western caldera

The shape of the low-velocity anomaly at ~1 km is comparable with that retrieved by gravity and magnetic fields data analysis in the past (Florio et al., 1999); especially in its northern boundary it spatially corresponds to an alignment of maxima obtained by using these techniques in the offshore caldera. This correlation suggests that a similar boundary may be present offshore, on the SW side of the anomaly. Nevertheless, the resolution of the seismic tomography images is much lower offshore (De Siena et al., 2018), while the SAR measurements are of course missing.

The main evidence against the existence of a setting similar to that at Solfatara across the western onshore boundaries retrieved by THD and ANT techniques (e.g. Monte Nuovo, the location of the last eruption at CFc) is the absence of recorded seismicity between 0 and 2 km. This absence can be affected by the sparser distribution of station in the western caldera but agrees with the weaker volcanic activity, e.g., at Mofete, with respect to Solfatara. The only seismic activity of the last 15 years detected in the western caldera is the September 7th, 2012, magmatic swarm. The swarm was located at a depth of ~3 km (red circles in Fig. 6a) and at the boundary between the high-velocity anomaly at Monte Gauro and the low-velocity primary anomaly (De Siena et al., 2018). Its occurrence corresponded to a local increase in the shear stress, modelled by the inflation of a sill-shaped reservoir located a depth of 2.5–3.1 km (D'D' Auria et al., 2015). Considering this swarm, both the lower contrast in ANT velocities and the decrease in density of THD_w maxima across the western caldera can be interpreted as a marker of deeper magmatic dynamics. The rim of the caldera (Battaglia et al., 2008) and especially the residual of eruptive conduits created during the last eruption (Chiodini et al., 2015; De Siena et al., 2018) are structures that may hinder shallower magmatic propagation in the western caldera or dampen its deformation signals. Deeper maps (Figs. 5 and 2 s - ~ 2 km) show a more consistent agreement with deep deformation source models. Above these depth, the stress was mainly released in the eastern caldera in 2011–2013 as here fracturing and structural features allow for a better channeling of magmatic fluids towards surface (Calò and Tramelli, 2018; De Siena et al., 2018).

5. Conclusions

We present the first comparison of SAR and ANT interferometric images at CFc, in order to achieve relevant information about the subsurface structures and caldera dynamics. While InSAR measurements provide information on both the spatial and the temporal features of ground deformation, ANT yields independent structural seismic constraints necessary to correctly interpret the dynamics of deformation sources. A significant spatial correlation was identified between the ANT velocity contrasts and the THD_w maxima distribution under

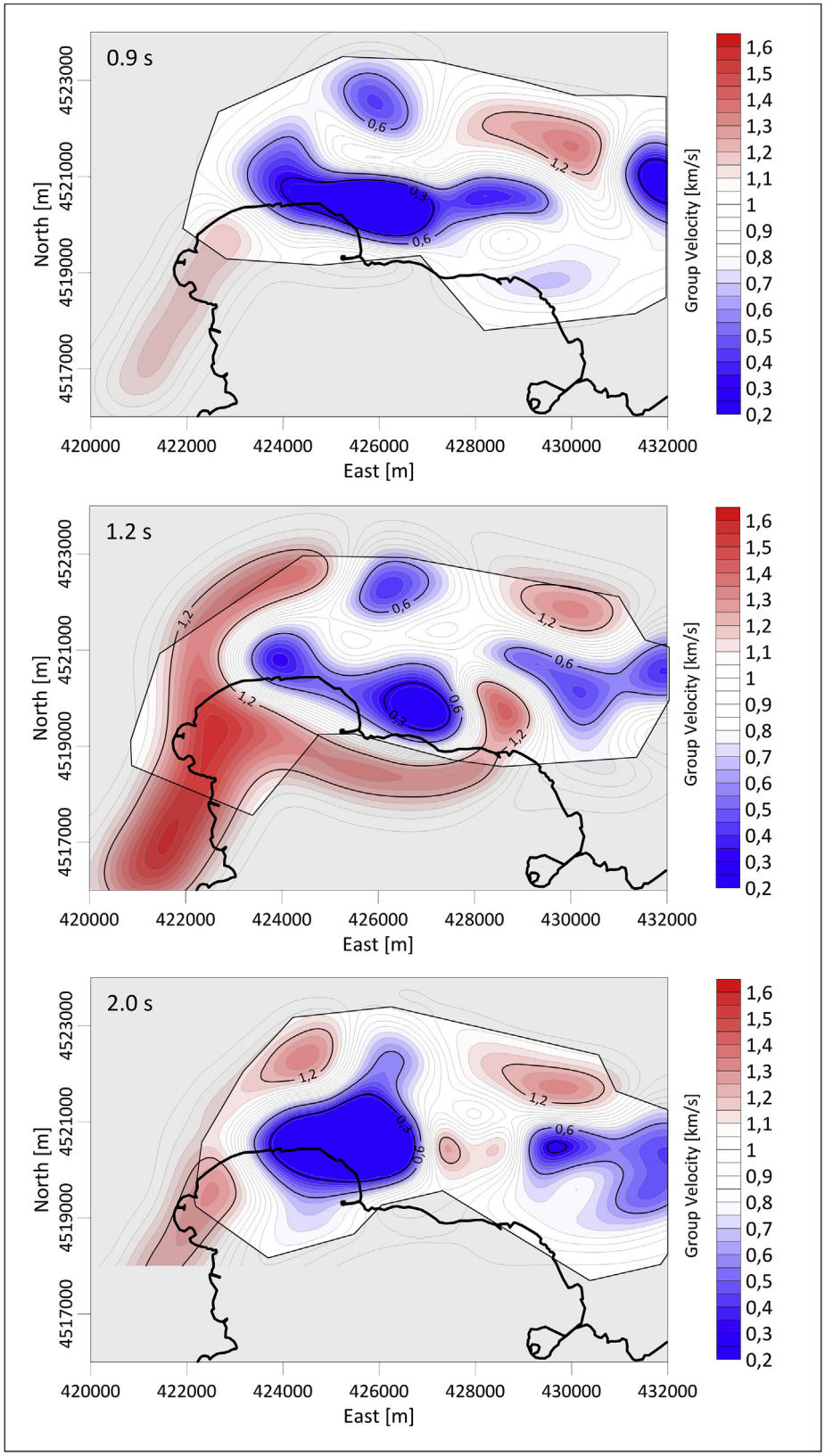

Fig. 5. ANT group-velocity model at different periods. Surface-wave (Rayleigh) group-velocity contour maps retrieved at different periods (0.9s, 1.2s, 2s) by the ANT analysis during the 2011–2013 unrest. The shaded polygon shows low-to-no resolution area.

Solfatara/Pisciarelli between May 2012 and March 2013, which InSAR data define as the main phase of deformation unrest. The comparison with both the spatial seismicity distribution between 2005 and 2013 and the patterns of extinct volcanic vents in the eastern caldera part (specifically at Solfatara/Pisciarelli and Astroni crater) demonstrate that these boundaries are dynamically active, with seismicity

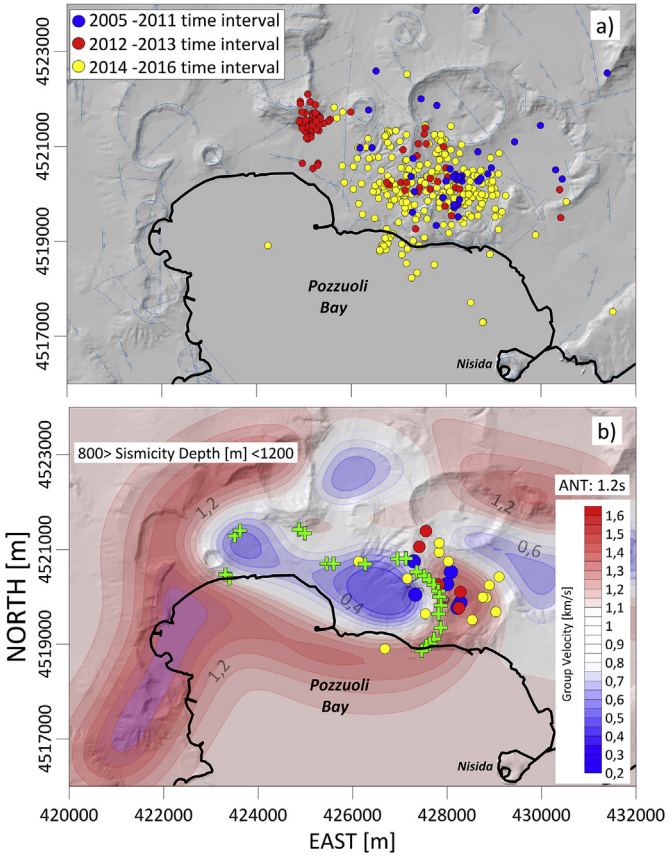

Fig. 6. 2005–2016 seismicity and SAR vs Seismic Interferometry. (a) Epicentral distribution of local seismicity relevant to the three temporal steps reported in Fig. 1. (b) Comparison between the maxima of THD_w (green crosses) and the 1.2 s period (~1 km depth) seismic velocity contour map with the 2005–2011 (blue circles), 2012–2013 (red circles), 2014–2016 (yellow circles) earthquake distributions between 800 *m* and 1200 *m* of depth. (For interpretation of the references to color in this figure legend, the reader is referred to the Web version of this article.)

concentrated at ~1 km to the east of the boundary. We infer that the imaged ANT velocity contrasts constrain the dynamics of the deformation source and the propagation of the magmatic intrusion within a sill-like structure also channeling the eastward propagation of magmatic fluids. Both the absence of seismicity in the first 2 km of the crust and fading of the THDw maxima suggest that magma and/or hydrothermal dynamic is less active in the western side of CFc.

Our work shows the importance of imaging shallow lateral heterogeneities when modelling the ground deformation patterns. Indeed, secondary structural effects may amplify local deformation in the early stage of an unrest: these signals can be mistakenly defined as early signs of impending eruptions (Del Gaudio et al., 2009). Accordingly, the importance of these structural effects should not be underestimated when interpreting geodetic data, modelling deformation sources or in the design of future monitoring networks. The joint exploitation of the InSAR measurements and seismic data revealed to be an excellent option to better understand the nature and the spatio-temporal pattern of the ground deformation source(s) at CFc. A combined application of InSAR and seismic tomography techniques like the one proposed here can provide a new perspective to understand the origin of deformation signal at other volcanoes, especially in calderas where magma propagation is expected to occur preferentially within sills.

Author contributions

S.P., L.D.S. and P.T. conceived the research; L.D.S., M.R.M, S.P., F.C. performed the seismic interferometry and SAR data processing and analysis. L. D, F.B. performed the seismic data analysis. R.C., A.B., M.F. and P.T. developed and applied the THD to the ground deformation field achieved by processed InSAR measurements. All authors co-wrote and reviewed the manuscript.

Conflicts of interest

No conflict of interest.

Acknowledgments:

This work was supported by the IREA-CNR/Italian Civil Defense Protection Department and the IREA-CNR/Italian Ministry of Economic Development DGS-UNMIG agreements; partially supported by DTA. AD004.065.001 Geophysics Project CNR _PDGP 2016–2019, by the "TFmicrosismicidad-magnetotelúrica (PTQ-15-08032) project, co-financed by the Torres Quevedo Program of the R&D Spanish National Plan 2013–2016". Moreover, we acknowledge the Scottish Alliance for Geosciences and Society (SAGES) for granting De Siena a Postdoctoral and Early Career Researcher Exchanges (PECRE) grant, used to develop most of the seismic analyses developed in this study". We thank Maurizio Battaglia, Ciro del Negro and the anonymous Reviewer for their very valuable suggestions.

References

Amoruso, A., Crescentini, L., Berrino, G., 2008. Simultaneous inversion of deformation and gravity changes in a horizontally layered half-space: evidences for magma intrusion during the 1982-1984 unrest at Campi Flegrei caldera (Italy). Earth Planet. Sci. Lett. 272, 181–188.

Amoruso, A., Crescentini, L., Sabbetta, I., 2014. Paired deformation sources of the Campi Flegrei caldera (Italy) required by recent (1980–2010) deformation history. J. Geophys. Res.: Solid Earth 119 (2), 858–879.

Ardhuin, F., Stutzmann, E., Schimmel, M., Mangeney, A., 2011. Ocean wave sources of seismic noise. J. Geophys. Res.: Oceans 116 (C9).

Aster, R.C., Meyer, R.P., 1988. Three-dimensional velocity structure and hypocenter distribution in the Campi Flegrei caldera, Italy. Tectonophysics 149 (3–4), 195–218.

Barone, A., Fedi, M., Tizzani, P., Castaldo, R., 2019. Multiscale Analysis of DInSAR measurements for multi-source investigation at uturuncu volcano (Bolivia). Remote Sens. 11, 703.

Battaglia, M., Gottsmann, J., Carbone, D., Fernandez, J., 2008. 4D volcano gravimetry. Geophysics 73 (6).

Berardino, P., Fornaro, G., Lanari, R., Sansosti, E., 2002. A new algorithm for surface deformation monitoring based on small baseline differential SAR interferograms. IEEE Trans. Geosci. Remote Sensing of Environment 40, 2375–2383.

Blakely, R.J., 1996. Potential Theory in Gravity and Magnetic Applications. Cambridge University Press, Cambridge, UK.

Borgia, A., Tizzani, P., Solaro, G., Manzo, M., Casu, F., Luongo, G., Pepe, A., Berardino, P., Fornaro, G., Sansosti, E., Ricciardi, G.P., Fusi, N., Di Donna, G., Lanari, R., 2005. Volcanic spreading of Vesuvius, a new paradigm for interpreting its volcanic activity. Geophys. Res. Lett. 32 (3), 1–4.

Brenguier, F., Shapiro, N.M., Campillo, M., Nercessian, A., Ferrazzini, V., 2007. 3-D surface wave tomography of the Piton de la Fournaise volcano using seismic noise correlations. Geophys. Res. Lett. 34 (2).

Bürgmann, R., Rosen, P.A., Fielding, E.J., 2000. Synthetic aperture radar interferometry to measure Earth's surface topography and its deformation. Annu. Rev. Earth Planet Sci. 28 (1), 169–209.

Calò, M., Tramelli, A., 2018. Anatomy of the Campi Flegrei caldera using enhanced seismic tomography models. Sci. Rep. 8 (1), 16254.

Castaldo, R., D'Auria, L., Pepe, S., Solaro, G., De Novellis, V., Tizzani, P., 2018a. The impact of crustal rheology on natural seismicity: Campi Flegrei caldera case study. Geosci. Front. https://doi.org/10.1016/j.gsf.2018.02.003.

Castaldo, R., Barone, A., Fedi, M., Tizzani, P., 2018b. Multiridge method for studying ground-deformation sources: application to volcanic environments. Sci. Rep. 8, 13420. https://doi.org/10.1038/s41598-018-31841-4.

Castaldo, R., Gola, G., Santilano, A., De Novellis, V., Pepe, S., Manzo, M., Manzella, A., Tizzani, P., 2017. The role of thermo-rheological properties of the crust beneath Ischia island (Southern Italy) in the modulation of the ground deformation pattern. J. Volcanol. Geotherm. Res. https://doi.org/10.1016/j.jvolgeores.2017.03.003.

Chiodini, G., Vandemeulebrouck, J., Caliro, S., D'Auria, L., De Martino, P., Mangiacapra, A., Petrillo, Z., 2015. Evidence of thermal-driven processes triggering the 2005–2014 unrest at Campi Flegrei caldera. Earth Planet. Sci. Lett. 414, 58–67.

Curtis, A., Gerstoft, P., Sato, H., Snieder, R., Wapenaar, K., 2006. Seismic interferometry—turning noise into signal. Lead. Edge 25 (9), 1082–1092.

D'Auria, L., Giudicepietro, F., Aquino, I., Borriello, G., Del Gaudio, C., Lo Bascio, D., et al., 2011. Repeated fluid-transfer episodes as a mechanism for the recent dynamics of

Campi Flegrei caldera (1989–2010). J. Geophys. Res.: Solid Earth 116 (B4).
D' Auria, L., Pepe, S., Castaldo, R., Giudicepietro, F., Macedonio, G., Ricciolino, P., Tizzani, P., Casu, F., Lanari, R., Manzo, M., Martini, M., Sansosti, E., Zinno, I., 2015. Magma injection beneath the urban area of Naples: a new mechanism for the 2012–2013 volcanic unrest at Campi Flegrei caldera. Sci. Rep. 5, 13100.
Del Gaudio, C., Aquino, I., Ricco, C., Serio, C., 2009. Monitoraggio geodetico dell'area vulcanica napoletana: risultati della livellazione geometrica di precisione eseguita ai Campi Flegrei a settembre 2008. Quad. Geofis. 66 (ISSN 1590-2595).
Del Negro, C., Currenti, G., Solaro, G., Greco, F., Pepe, A., Napoli, R., Pepe, S., Casu, F., Sansosti, E., 2013. Capturing the fingerprint of Etna volcano activity in gravity and satellite radar data. Sci. Rep. 3, 3089.
De Novellis, V., Castaldo, R., De Luca, C., Pepe, S., Zinno, I., Casu, F., Lanari, R., Solaro, G., 2017. Source modelling of the 2015 Wolf volcano (Galápagos) eruption inferred from Sentinel 1-A DInSAR deformation maps and pre-eruptive. J. Volcanol. Geotherm. Res. 344, 246–256. https://doi.org/10.1016/j.jvolgeores.2017.05.013.
De Siena, L., Del Pezzo, E., Bianco, F., 2010. Seismic attenuation imaging of Campi Flegrei: evidence of gas reservoirs, hydrothermal basins, and feeding systems. J. Geophys. Res.: Solid Earth 115https://doi.org/10.1029/2009JB006938. B09312, 18 pp.
De Siena, L., Amoruso, A., Del Pezzo, E., Wakeford, Z., Castellano, M., Crescentini, L., 2017a. Space-weighted seismic attenuation mapping of the aseismic source of Campi Flegrei 1983–84 unrest. Geophys. Res. Lett. 44 (4), 1740–1748.
De Siena, L., Chiodini, Giovanni, Vilardo, Giuseppe, Del Pezzo, Edoardo, Castellano, Mario, Colombelli, Simona, Tisato, Nicola, Ventura, Guido, 2017b. Source and dynamics of a volcanic caldera unrest: Campi Flegrei, 1983–84. Sci. Rep. 7, 8099.
De Siena, L., Sammarco, C., Cornwell, D.G., La Rocca, M., Bianco, F., Zaccarelli, L., Nakahara, H., 2018. Ambient seismic noise image of the structurally-controlled heat and fluid feeder pathway at Campi Flegrei caldera. Geophys. Res. Lett. 45 (13), 6428–6436 2018.
Di Luccio, F., Pino, N.A., Piscini, A., Ventura, G., 2015. Significance of the 1982–2014 Campi Flegrei seismicity: preexisting structures, hydrothermal processes, and hazard assessment. Geophys. Res. Lett. 42 (18), 7498–7506.
Fedi, M., Florio, G., 2001. Detection of potential fields source boundaries by enhanced horizontal derivative method. Geophys. Prospect. 49, 40–58.
Fernandez, J., Tizzani, P., Manzo, M., Borgia, A., Gonzalez, P.J., Marti, J., Pepe, A., Camacho, A.G., Casu, F., Berardino, P., Prieto, J.F., Lanari, R., 2009. Gravity-driven deformation of Tenerife measured by InSAR time series analysis. Geophys. Res. Lett. 36 (4) art. no. L04306.
Ferretti, A., Prati, C., Rocca, F., 2001. Permanent scatterers in SAR interferometry. IEEE Trans. Geosci. Remote Sens. 39 (1), 8–20.
Florio, G., Fedi, M., Cella, F., Rapolla, A., 1999. The Campanian Plain and Phlegrean Fields: structural setting from potential field data. J. Volcanol. Geotherm. Res. 91, 361–379.
Franceschetti, G., Lanari, R., 1999. Synthetic Aperture Radar Processing. CRC Press, Boca Raton (FL.
Gabriel, A.K., Goldstein, R.M., Zebker, H.A., 1989. Mapping small elevation changes over large areas: differential interferometry. J. Geophys. Res. 94 (B7), 9183–9191.
Garnier, J., Papanicolaou, G., 2016. Passive Imaging with Ambient Noise. Cambridge University Press, Cambridge, UK.
Giudicepietro, F., Macedonio, G., D'Auria, L., Martini, M., 2016. Insight into vent opening probability in volcanic calderas in the light of a sill intrusion model. Pure Appl. Geophys. 173 (5), 1703–1720.
Hooper, A., Zebker, H., Segall, P., Kampes, B.M., 2014. A new method for measuring deformation on volcanoes and other natural terrains using InSAR persistent scatterers. Geophys. Res. Lett. 31 (23), L23611-1–L23611-5.
Isaia, R., Vitale, S., Di Giuseppe, M.G., Iannuzzi, E., Tramparulo, F.D.A., Troiano, A., 2015. Stratigraphy, structure, and volcano-tectonic evolution of Solfatara maar-diatreme (Campi Flegrei, Italy). GSA Bulletin 127 (9–10), 1485–1504.
Jaxybulatov, K., Shapiro, N.M., Koulakov, I., Mordret, A., Landès, M., Sens-Schönfelder, C., 2014. A large magmatic sill complex beneath the Toba caldera. Science 346 (6209), 617–619.
Koulakov, I., Vargas, C.A., 2018. Evolution of the magma conduit beneath the Galeras volcano inferred from repeated seismic tomography. Geophys. Res. Lett. 45 (15), 7514–7522.
Lanari, R., De Natale, G., Berardino, P., Sansosti, E., Ricciardi, G.P., Borgstrom, S., Capuano, P., Pingue, F., Troise, C., 2002. Evidence for a peculiar style of ground deformation inferred at Vesuvius volcano. Geophys. Res. Lett. 29 (9). https://doi.org/10.1029/2001GL014571.
Lecocq, T., Caudron, C., Brenguier, F., 2014. MSNoise, a python package for monitoring seismic velocity changes using ambient seismic noise. Seismol. Res. Lett. 85 (3), 715–726.
Li, J., Heap, A.D., 2008. A Review of Spatial Interpolation Methods for Environmental Scientists. Geoscience Australia, Canberra, Australia.
Luiso, P., Paoletti, V., Nappi, R., La Manna, M., Cella, F., Gaudiosi, G., Fedi, M., Iorio, M., 2018. A multidisciplinary approach to characterize the geometry of active faults: the example of Mt. Massico, Southern Italy. Geophys. J. Int. 213 (3), 1673–1681. https://doi.org/10.1093/gji/ggy080.
Manconi, A., Walter, T.R., Manzo, M., Zeni, G., Tizzani, P., Sansosti, E., Lanari, R., 2010. On the effects of 3-D mechanical heterogeneities at Campi Flegrei caldera, southern Italy. JGR Solid Earth 115 (B8).
Manzo, M., Ricciardi, G.P., Casu, F., Ventura, G., Zeni, G., Borgstrom, S., Berardino, P., Del Gaudio, C., Lanari, R., 2006. Surface deformation analysis in the Ischia island (Italy) based on spaceborne radar interferometry. J. Volcanol. Geotherm. Res. 151, 399–416. https://doi.org/10.1016/j.jvolgeores.2005.09.010.
Massonnet, D., Feigl, K.L., 1998. Radar interferometry and its application to changes in the Earth's surface. Rev. Geophys. 36 (4), 441–500.
Masterlark, T., Feigl, K.L., Haney, M., Stone, J., Thurber, C., Ronchin, E., 2012. Nonlinear estimation of geometric parameters in FEMs of volcano deformation: integrating tomography models and geodetic data for Okmok volcano, Alaska. J. Geophys. Res. 117, B02407.
Masterlark, T., Donovan, T., Feigl, K.L., Haney, M., Thurber, C.H., Tung, S., 2016. Volcano deformation source parameters estimated from InSAR: sensitivities to uncertainties in seismic tomography. J. Geophys. Res. Solid Earth 121, 3002–3016.
Mattia, M., Bruno, V., Caltabiano, T., Cannata, A., Cannavò, F., D'Alessandro, W., Di Grazia, G., Federico, C., Gianmarco, S., La Spina, A., Liuzzo, M., Longo, M., Monaco, C., Patanè, D., Salerno, G., 2015. A comprehensive interpretative model of slow slip events on Mt. Etna's eastern flank. Geochem. Geophys. Geosyst. 16 (3), 635–658.
Mora, O., Mallorquí, J.J., Broquetas, A., 2003. Linear and nonlinear terrain deformation maps from a reduced set of interferometric SAR images. IEEE Trans. Geosci. Remote Sens. 41 (10), 2243–2253.
Nagaoka, Y., Nishida, K., Aoki, Y., Takeo, M., Ohminato, T., 2012. Seismic imaging of magma chamber beneath an active volcano. Earth Planet. Sci. Lett. 333, 1–8.
Obermann, A., Planes, T., Larose, E., Campillo, M., 2013. Imaging pre-eruptive and coeruptive structural and mechanical changes of a volcano with ambient seismic noise. J. Geophys. Res.: Solid Earth 118 (12), 6285–6294.
Orsi, G., Civetta, L., Del Gaudio, C., De Vita, S., Di Vito, M.A., Isaia, R., Petrazzuoli, S.M., Ricciardi, G.P., Ricco, C., 1999. Short-term ground deformations and seismicity in the resurgent Campi Flegrei caldera (Italy): an example of active block-resurgence in a densely populated area. J. Volcanol. Geotherm. Res. 91 (2–4), 415–451 1999.
Pepe, A., Sansosti, E., Berardino, P., Lanari, R., 2005. On the generation of ERS/ENVISAT DInSAR time-series via the SBAS technique. IEEE Geosci. Remote Sens. Lett. 2 (3), 265–269.
Pepe, S., Castaldo, R., De Novellis, V., D'Auria, L., De Luca, C., Casu, F., Sansosti, E., Tizzani, P., 2017. New insights on the 2012–2013 uplift episode at fernandina volcano (galapagos). Geophys. J. Int. 211, 673–685.
Pepe, S., D'Auria, L., Castaldo, R., Casu, F., De Luca, C., De Novellis, V., Sansosti, E., Solaro, G., Tizzani, P., 2018. The use of massive deformation datasets for the analysis of spatial and temporal evolution of mauna loa volcano (Hawai'i). Remote Sens. 10 (6), 968.
Reuber, G.S., Kaus, B.J.P., Popov, A.A., Baumann, T.S., 2018. Unraveling the Physics of the Yellowstone Magmatic System Using Geodynamic Simulations. Front. Earth Sci. 6, 117.
Ridsdill-Smith, T.A., 1999. Wavelet Design of Time-Varying Filters. In: Proceedings of the Fifth International Symposium on Signal Processing and its Applications, Brisbane, QLD, Australia, 22–25 August 1999.
Sens-Schönfelder, C., Wegler, U., 2006. Passive image interferometry and seasonal variations of seismic velocities at Merapi Volcano, Indonesia. Geophys. Res. Lett. 33 (21).
Serlenga, V., de Lorenzo, S., Russo, G., Amoroso, O., Garambois, S., Virieux, J., Zollo, A., 2016. A three-dimensional QP imaging of the shallowest subsurface of Campi Flegrei offshore caldera, southern Italy. Geophys. Res. Lett. 43 (21), 11–209.
Shapiro, N.M., Campillo, M., Stehly, L., Ritzwoller, M.H., 2005. High-resolution surface-wave tomography from ambient seismic noise. Science 307 (5715), 1615–1618.
Solaro, G., Acocella, V., Pepe, S., Ruch, J., Neri, M., Sansosti, E., 2010. Anatomy of an unstable volcano from InSAR: multiple processes affecting flank instability at Mt. Etna, 1994-2008. J. Geophys. Res. 115 (B10). https://doi.org/10.1029/2009JB000820, 2010. 405.
Tizzani, P., Berardino, P., Casu, F., Euillades, P., Manzo, M., Ricciardi, G.P., Zeni, G., Lanari, R., 2007. Surface deformation of Long Valley caldera and Mono Basin, California, investigated with the SBAS-InSAR approach. Remote Sens. Environ. 108 (3), 277–289.
Tizzani, P., Battaglia, M., Zeni, G., Atzori, S., Berardino, P., Lanari, R., 2009. Uplift and magma intrusion at Long Valley caldera from InSAR and gravity measurements. Geology 37 (1), 63–66.
Tizzani, P., Manconi, A., Zeni, G., Pepe, A., Manzo, M., Camacho, A., Fernandez, J., 2010. Long-term versus short-term deformation processes at Tenerife (Canary Islands). J. Geophys. Res. 115 (B12) 412.
Tizzani, P., Battaglia, M., Castaldo, R., Pepe, A., Zeni, G., Lanari, R., 2015. Magma and fluid migration at Yellowstone Caldera in the last three decades inferred from InSAR, leveling and gravity measurements. J. Geophys. Res. Solid Earth 120, 2627–2647.
Trasatti, E., Casu, F., Giunchi, C., Pepe, S., Solaro, G., Tagliaventi, S., Berardino, P., Manzo, M., Pepe, A., Ricciardi, G.P., Sansosti, E., Tizzani, P., Zeni, G., Lanari, R., 2008. The 2004-2006 uplift episode at Campi Flegrei caldera (Italy): Constraints from SBAS-DInSAR ENVISAT data and Bayesian source inference. Geophys. Res. Lett. 35 (7).
Vanorio, T., Virieux, J., Capuano, P., Russo, G., 2005. Three-dimensional seismic tomography from P wave and S wave microearthquake travel times and rock physics characterization of the Campi Flegrei Caldera. J. Geophys. Res.: Solid Earth 110 (B3).
Vilardo, G., Isaia, R., Ventura, G., De Martino, P., Terranova, C., 2010. InSAR Permanent Scatterer analysis reveals fault re-activation during inflation and deflation episodes at Campi Flegrei caldera. Remote Sens. Environ. 114 (10), 2373–2383.
Vitale, S., Isaia, R., 2014. Fractures and faults in volcanic rocks (Campi Flegrei, southern Italy): insight into volcano-tectonic processes. Int. J. Earth Sci. 103 (3), 801–819.
Wapenaar, K., Fokkema, J., 2006. Green's function representations for seismic interferometry. Geophysics 71 (4), SI33–SI46.
Wright, T.J., Lu, Z., Wicks, C., 2003. Source model for the Mw 6.7, 23 October 2002, Nenana Mountain Earthquake (Alaska) from InSAR. Geophys. Res. Lett. 30 (18). https://doi.org/10.1029/2003GL018014. 1974.
Zollo, A., Judenherc, S., Auger, E., D'Auria, L., Virieux, J., Capuano, P., et al., 2003. Evidence for the buried rim of Campi Flegrei caldera from 3-d active seismic imaging. Geophys. Res. Lett. 30 (19).